FLEXURAL STRENGTH AND NUMERICAL SIMULATION OF ASR AFFECTED BEAMS

Saeid Hajighasemali[1,*], Ali Akbar Ramezanianpour[2], Vahid Lotfi[2]

[1]Faculty member of Islamic Azad University, Roudehen branch, TEHRAN, Iran

[2]Professor of Amirkabir University of Technology, Dept. of Civil Engineering, TEHRAN, Iran

Abstract

Alkali silica reaction is the reaction between alkali in cement and certain forms of silica in aggregates. The reaction produces gel resulting in cracking and disintegration of concrete.

A laboratory study was carried out to investigate the effect of deleterious ASR expansion on the structural behavior of reinforced concrete beams. The specimens were made with reactive or non-reactive aggregates. All beams had 100×150×1100 mm dimensions and internal reinforcement. After loading, specimens were kept under long-term observation at $38^{\circ}C$ and 100 percent relative humidity.

It was quite clear that the beams containing reactive aggregate showed a significant increasing strain. Ultimate loads are reduced in ASR affected beams due to large irreversible steel strains.

A method was used to model ASR strains and creep strains for this research by the finite element program ANSYS. The comparison reveals that finite element models have good agreement with acquired test results.

Keywords: Alkali silica reaction (ASR); Expansion; Reinforced concrete beams; Flexural strength; Finite element method

1 INTRODUCTION

Many structures, such as dams, bridges and hydraulic structures, are suffering from deterioration due to alkali silica reaction (ASR) that impair durability and might also affect the safety of installations. Some researchers investigated beams affected by ASR [1, 2, 3, 4, 5, 6, 8]. In all researches, ASR created large irreversible concrete and steel strains. But there are contradictory results of ASR effects on the overall serviceability, strength and stability of structural concrete members. In an investigation, ASR affected beams under load exhibited considerable losses of flexural strength [1]. Other researches indicated that even though the reactive reinforced beams experienced visible cracking due to ASR, their flexural loading capacity was nearly the same as that of the non-reactive aggregate beams [2,5]. However, few researches showed that ASR increased the shear capacity of reinforced concrete beams [3]. This paper focuses on the new results obtained from the effects of ASR on flexural behavior of reinforced concrete beams.

2 EXPERIMENTAL PROGRAM

2.1 Constituent materials

Type II Portland cement in accordance with ASTM C1260 standard [9] was used. Aggregates used in Ostoor dam were selected as reactive aggregates.

This aggregate has been confirmed to be reactive by the accelerated mortar-bar ASTM C1260 test method. Figure 1 shows that the expansion in both fine and coarse aggregates has exceeded the maximum allowable value of 0.2 percent. For comparison purposes, a non-reactive aggregate was selected. The result of mortar-bar test is shown in Figure 2.

The measured value of the yield strength of the ribbed bar was about 370 MPa.

2.2 Test specimens

Two concrete mixtures were produced. The first mixture was prepared with reactive aggregates and the second mixture had non-reactive ones.

Fourteen 1100mm long reinforced concrete beams were made; seven with the reactive aggregates concrete indicated by R.t.c , and seven with non-reactive aggregates concrete indicated by

* Correspondence to: saeid1352@yahoo.com

N.t.c with t the bar diameter at the tension side and c the bar diameter at the compressive side. For example beam R.8.0 should be read as reactive concrete mix with 8 mm bar at tension side and no bar at compressive side or beam N.12.8 should be read as non-reactive concrete mix with 12 mm bar at tension side and 8 mm bar at compressive side. All beams had a 100×150mm rectangular cross section and were provided with stirrups. Details of the beams are shown in Figure 3.

In addition, 100×100mm and 150×300 mm concrete cylinders having similar mixture proportion of the concrete in the beams were also cast. The average strengths of the reactive and non-reactive aggregates concretes at 28 days were 25.6 and 26.2 MPa, respectively. The test specimens were kept in the moulds for 1 day. After demolding, the specimens were moist cured. For length expansion measurements, studs were glued to the specimens as shown in Figure 4. A strain gauge was mounted on the middle of each bar for monitoring steel strains.

2.3 Loading condition

To investigate the ASR expansion of beams while under simulated service loads, seven pairs of identical beams, one with reactive aggregates and one with non-reactive aggregates, were loaded. Details of loading system are shown in Figure 5. Two steel blocks with dimensions of 40×40×150 mm were placed about 333mm apart in the center between the two beams. The loading was gradually increased by fastening the nuts on the steel rods until cracks having a width of about 0.2mm were observed on the tension face of the beams. During the loading period, the applied load was checked regularly by measuring the steel strain using Demec studs installed on the rods, and adjusted if necessary.

2.4 ASR accelerated conditioning

The Na_2O_{eq} content in the concrete mixture was increased to 1.75% of the cement weight for reactive aggregate beams by adding sodium hydroxide solution into the mixing water.

A tank having dimensions of 600×600×3600mm was used for ASR accelerated conditioning.

All specimens except one of the two beams R.12.8 and one of the two beams N.12.8 were placed in the tank. In order to obtain 100 percent relative humidity, 60 mm depth of water was kept at the bottom of the tanks. The temperature of the water was raised to $38^{\circ}C$ by a temperature-controlled heater.

2.5 Creep strain measurement

For creep strain measurements, two R.12.8 and two N.12.8 beams were manufactured. Two pairs of beams, one of each series, were loaded and one of them was placed in a tank and the other at controlled laboratory conditions. The concrete and steel strains of the beams were regularly monitored. Difference between the strains of the two beams N.12.8 is due to the increase in the temperature and moisture absorption of the beam which was in the tank. In order to calculate the creep strain in non-reactive aggregate beams, this difference was subtracted from the strains of N.8.0 to N12.10 specimens.

3 TEST RESULTS AND DISCUSSION

The measured strains are divided into the following three major parts:

1) Service load strain: This strain is approximately similar for both reactive and non - reactive aggregate beams.
2) Creep strain: Creep of concrete increases the tension and compression strains in both reactive and non-reactive aggregate beams.
3) ASR strain: The length change due to ASR appears after 100 days only for reactive aggregate beams. It increases the tension strain but reduces the compression strain.

There is also minor increase in strains at initial days due to the increase in temperature and moisture absorption.

A schematic model of strain distribution is shown in Figure 6. The total measured strain is a combination of the elastic strain caused by the bending load, creep strain and tensile strain due to ASR. It is found from this figure that the neutral axis of the ASR affected beams has shifted towards the tension face at earlier ages due to creep, and towards the compression face at longer ages due to alkali- silica reaction. This is a very important structural implication indicating that the strain in the tension steel had also increased due to expansive gel formation.

3.1 ASR strain

In order to obtain ASR Strain, the strains of non-reactive aggregate beams were subtracted from the strains of reactive aggregate beams. Concrete ASR strains are shown in Figures 7 and 8. It is clear that the ASR strain in compression zone is higher than that of tension zone because of higher restraint of the tension reinforcement.

3.2 Mechanical tests of concrete cylinders

Expansion of reactive and non-reactive aggregate concrete cylinders is shown in Figure 9. After 240 days, the strain in the reactive aggregate concrete cylinder has reached to about 1050 micro-strain. Compressive strength and non-destructive dynamic modulus tests in accordance with ASTM C215-91 test method were carried out at laboratory conditions [7]. The variations of compressive strength and dynamic modulus of elasticity of concretes are shown in Figure 10. It was found that the variation in the mechanical properties was related to the ASR expansion. The compressive strength and dynamic modulus were not affected significantly up to 100 days. At the age of 240 days, the losses in the compressive strength and dynamic modulus of the concrete cylinders were 28 and 34 percent respectively compared with the corresponding 28 day values.

4 CONCRETE BEAMS FLEXURAL LOADING

After 270 days of ASR accelerated conditioning with sustained load, flexural loading tests were carried out to investigate the structural behavior of the reinforced concrete beams (Figure 11). Deflections at the first point of the beams were measured using Linear Variable Differential Transformer (LVDT). The beams were loaded symmetrically at two points with 1000 mm span until concrete crushing occurred near the top face of the compression zone. During the test the total force was recorded. Results of the tests are shown in Figures 12 to 17. It can be seen that ASR reduces the stiffness of all concrete beams. The first crack load, reinforcement yielding load and the ultimate load are reduced in ASR affected beams due to large steel strains and reduction of the compressive strength due to ASR, especially for the unconfined concrete in compression zone. This reduced strength and probably also stiffness will result in a smaller internal lever arm and thus in a smaller bending moment at failure. Table 1 shows the first crack load, reinforcement yielding load and the failure load carried by the ASR-affected beams, and the percentage loss in these loads compared to the control beams. The important role of the compression steel is clear from the results. Increase in compression steel resulted in the reduction of the percentage loss of failure loads.

5 NUMERICAL SIMULATION OF BEAMS SUBJECTED TO ASR

The finite element mesh used for the simulation in ANSYS program is illustrated in Figure 18. Beams were divided into 1056 8-node brick elements.

The elastic modulus of steel bar is 210 GPa. The steel bar area at top and bottom are in accordance with the tests. Initial elastic modulus of concrete is 24.3 GPa. The concrete was modeled using Solid65 element and the reinforcements in two directions were modeled by Link element. Beams were loaded as Figure 11 with service load. Non-linear analysis with concrete cracking was used for solution techniques.

5.1 Internal Pressure due to ASR

The gel pressure is shown in Figure 19. This pressure is uniform and in all directions. When the circumferential tensile stress due to this internal pressure exceeds the tensile strength, cracks will occur in concrete around the gel. Then these cracks continue toward the surface of concrete when the gel pressure becomes higher. The internal pressure was calculated by ANSYS modelling of a beam without any reinforcement and restraint accordance to free expansion of concrete cylinder prisms. Then for each element the consistent equivalent nodal forces were utilized corresponding to these internal pressures (Figure 20).

5.2 Creep

Creep can be divided into two stages as shown in Figure 21[10]. During the primary creep stage the creep rate decreases to a certain value (minimum creep rate).The secondary stage is characterized by approximately constant creep rate. The primary creep and secondary creep were used in accordance with theories described in ANSYS theoretical manual [10].

5.3 Results and discussion

Figures 22 to 27 show the concrete strains obtained from numerical simulation and test results. It is clear from these figures that there are good agreements between experimental data and the model. The differences in tension strains for R.8.0 to R.12.10 beams in the model compared to test results are 26, 17, 17, 16, 16, 12 percent, respectively. In the compression zones, the program results can show the behavior of beams but differences between experiments and the model are more significant compared to tension zones. The differences in compression strains for R.8.0 to R.12.10 beams in the model compared to test results are 23, 19, 20, 18, 14, 10 percent respectively. It is found from these figures that using compression steel bar causes significant agreement between experimental and model results. In R.12.10 beam with highest compression steel bar, the differences between experimental results and the model results in tension and compression zones are 12 and 10 percent, respectively. These values for R.12.0 beam with no compression steel bar are 17 and 20 percent, respectively.

6 CONCLUSIONS

From the results obtained in this investigation, the following conclusions can be drawn:

- Expansion of ASR in tension zone of beams is less than in compression zone due to the higher restraint from the tension reinforcement
- The neutral axis of the beams shifted towards the compression face due to ASR.
- Due to large differences in concrete strains between the tension and compression zone of beams, influence of the increase in tension steel with constant compression steel is insignificant on compression zone.
- Influence of increase in compression steel with constant tension steel on tension zone is significant
- Mechanical properties of concrete cylinders are closely related to ASR expansion. At an age of 8 months, the compressive strength and dynamic modulus of elasticity were reduced by 28 and 34 percent respectively when compared with the corresponding 28-day values.
- ASR shows a much more detrimental effect on the mechanical properties and expansion of concrete cylinders than on the expansion of reinforced concrete beams due to confining the concrete by reinforcements in reinforced concrete beams.
- Due to large steel strains and reduction of the compressive strength due to ASR, especially for the unconfined concrete in compression zone, failure loads are reduced in ASR affected beams. Increase in compression steel, reduces percentage loss of failure load**.**
- Considering the ASR effect as an internal pressure, is a suitable method to model this phenomenon.

7 REFERENCES

[1] Swamy R.N., AL- Asali M.M. (1989): Effect of Alkali – Silica Reaction on the Structural Behavior of Reinforced Concrete Beams. ACI Structural Journal (86): 451-459.

[2] Shenfu F., Hanson J.M. (1998): Effect Of Alkali Silica Reaction Expansion And Crackig On Structural Behavior Of Reinforced Concrete Beam. ACI Structural Journal (95): 498 – 505.

[3] Ahmed T., Burley E., Rigden S. (1998): The Static And Fatigue Strength Of Reinforced Concrete Beams Affected By Alkali – Silica Reaction. ACI Material Journal (95): 376-388.

[4] Marzouk H., Langdon S. (2003): The Effect Of alkali-Aggregate Reactivity on The Mechanical Properties of High and Normal Strength Concrete. Cement And Concrete Composites (25): 549-556

[5] Multon S., Dubroca S., Seignol J.F., Toutlemonde F. (2004): Flexural Strength of Beams Affected By ASR. Proceedings of the 12th International Conference on Alkali-Aggregate Reaction in Concrete, China: 1181—1190.

[6] Shenfu F., Hanson J.M. (1998): Length Expansion and Cracking of Plain and Reinforced Concrete Prisms Due to Alkali-Silica Reaction. ACI Materials Journal (95): 480-487.

[7] ASTM C215-91 (1995): Standard Test Method for Fundamental Transverse, Longitudinal, and Torsional Frequencies of Concrete Specimens, Annual Book of ASTM Standards (04.02): 123-128.

[8] Hamada H., Swamy R., Laiw J. (2004): Influence of protective surface coating on the structural behaviour ASR affected RC beams under sustained loading. Proceedings of the 12th International Conference on Alkali-Aggregate Reaction in Concrete, China: 1235-1244.

[9] ASTM C1260 (1999): Standard Test Method for Potential Alkali Reactivity of Aggregates (Mortar – Bar Method), Annual Book of ASTM Standards (04.02): 650- 653.

[10] Naumenko. K. (2006): Modelling of high temperature creep for structural analysis applications, Ukraine.

TABLE 1: First crack load, Reinforcement yielding load and Failure load for ASR affected beams compared to control beams.

Beam No.	First crack load (kN)	Percentage loss compared to control beam	Reinforcement yielding load (kN)	Percentage loss compared to control beam	Failure load (kN)	Percentage loss compared to control beam
R.8.0	7	45.6	28	19	30	18.9
R.10.0	7.5	53.1	38	13.6	42	15
R.12.0	12	34	58	13.4	61.2	15
R.10.8	10.5	37.5	40	9	42.5	9.5
R.12.8	11	37.1	57	10.9	63	9
R.12.10	13.3	32.8	56	6.7	63.1	6.2

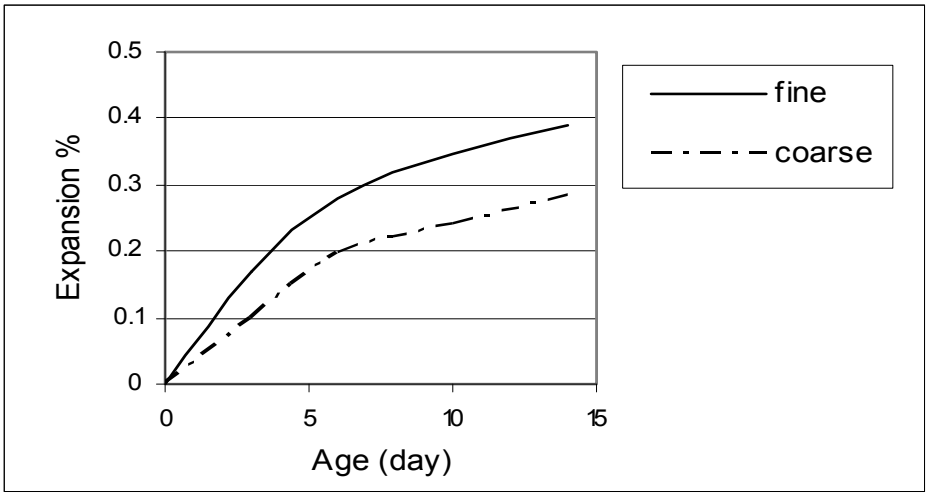

Figure 1: Accelerated mortar-bar testing for reactive aggregate.

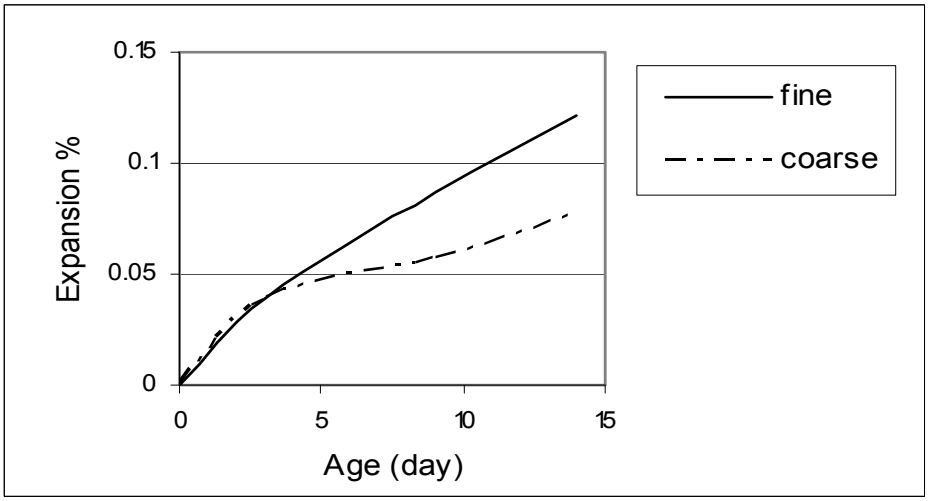

Figure 2: Accelerated mortar-bar testing for non-reactive aggregate.

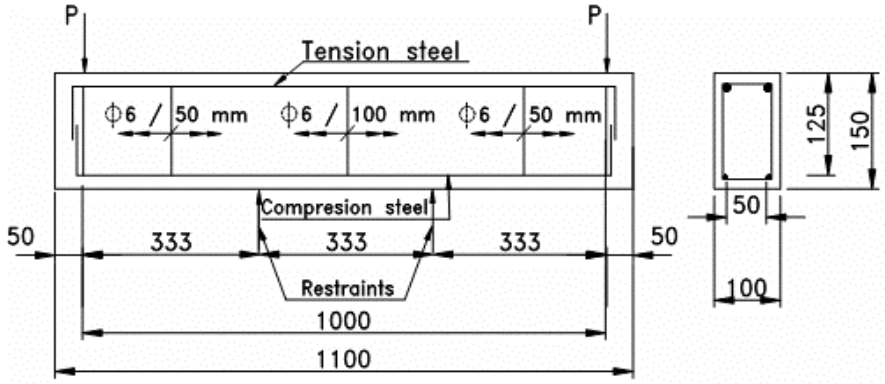

Figure 3: Reinforced concrete beams.

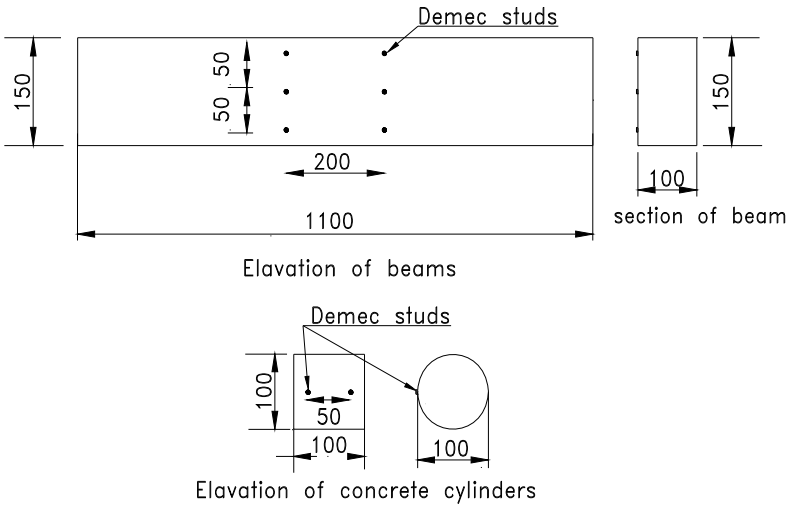

Figure 4: Arrangement of demec studs on specimens.

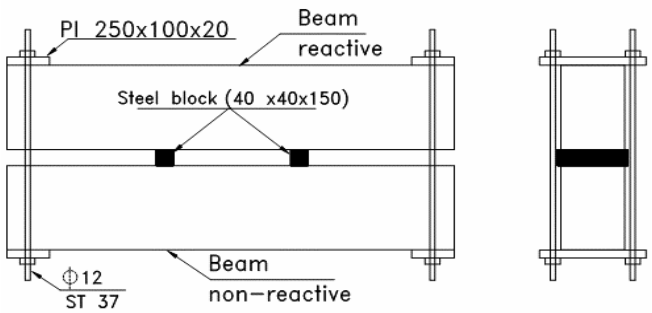

Figure 5: Details of loading.

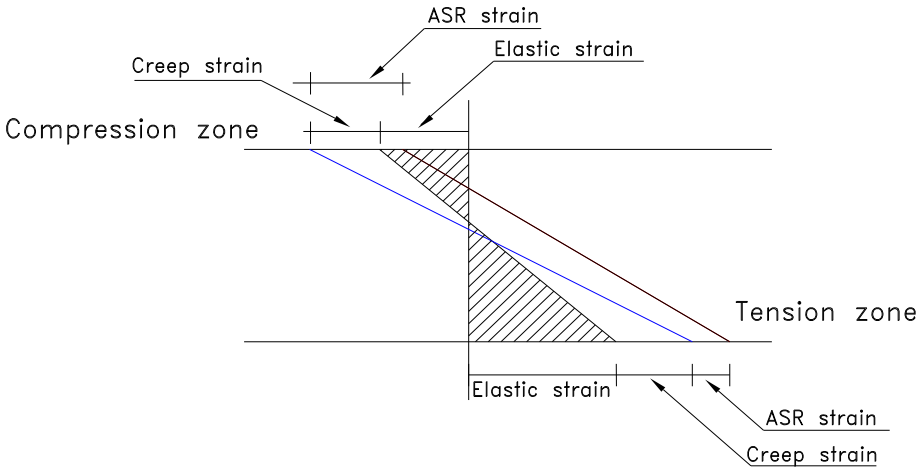

Figure 6: strain distribution.

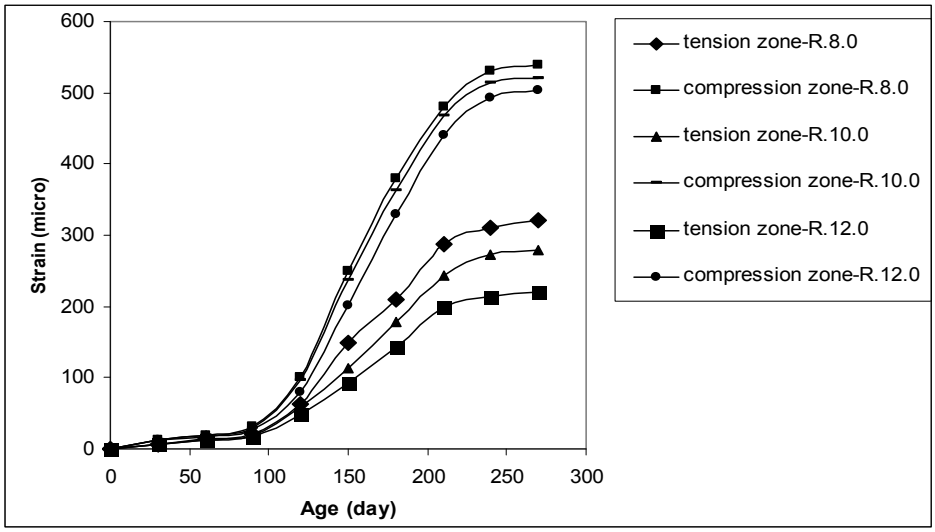

Figure 7: Concrete strains due to ASR in R.8.0, R.10.0, and R.12.0 beams.

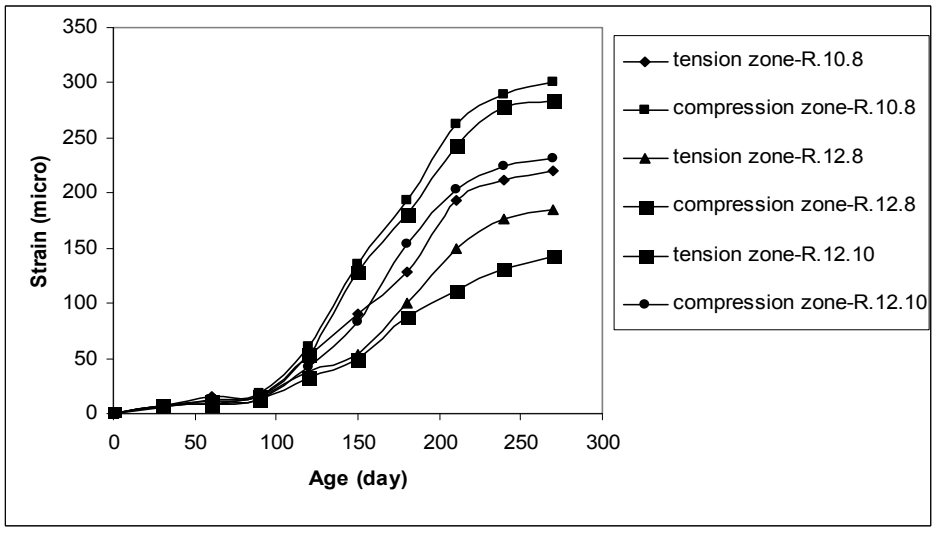

Figure 8: Concrete strains due to ASR in R.10.8, R.12.8, and R.12.10 beams.

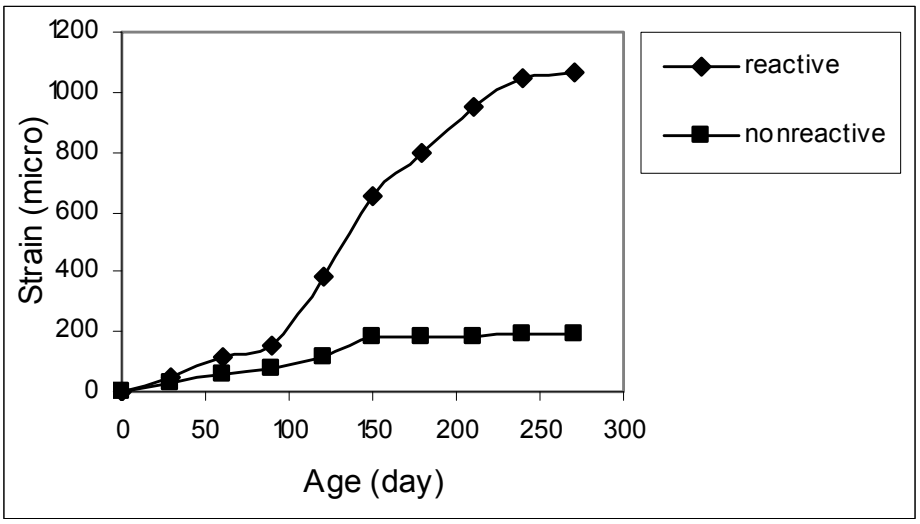

Figure 9: ASR strain of concrete cylinders.

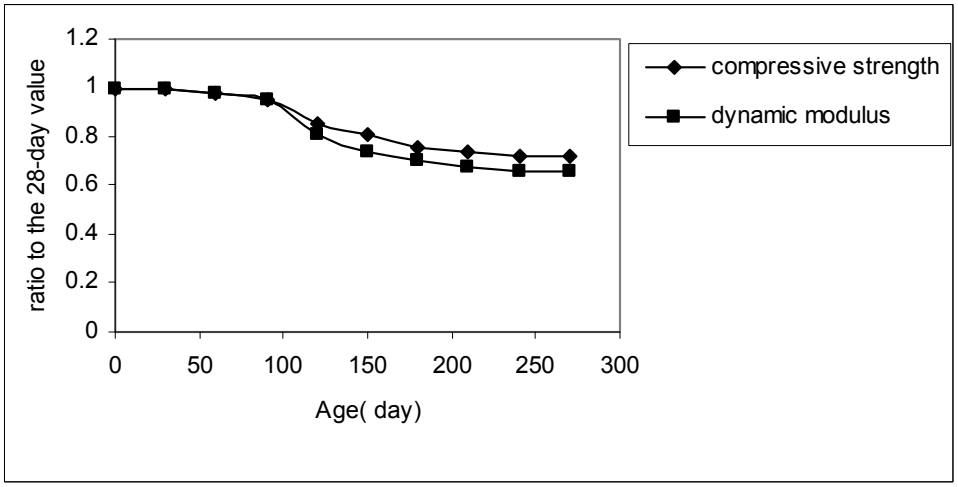

Figure 10: Change in mechanical properties of reactive concrete cylinders.

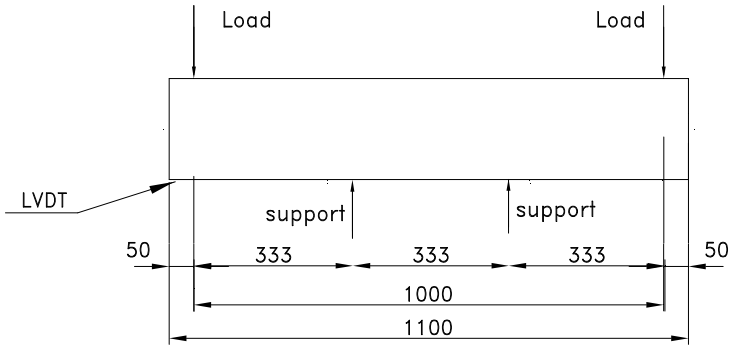

Figure 11: Beam setup for loading at both ends.

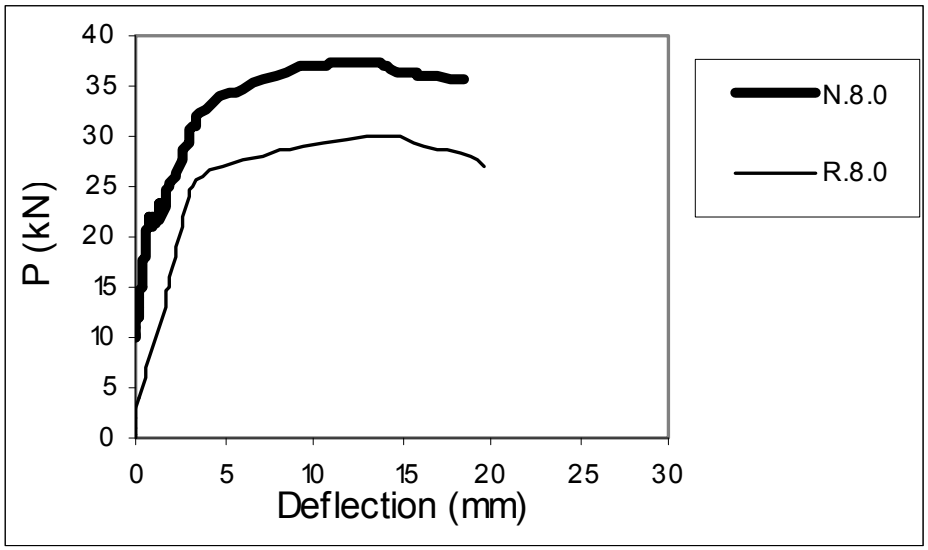

Figure 12: Load versus deflection for N.8.0 and R.8.0 beams.

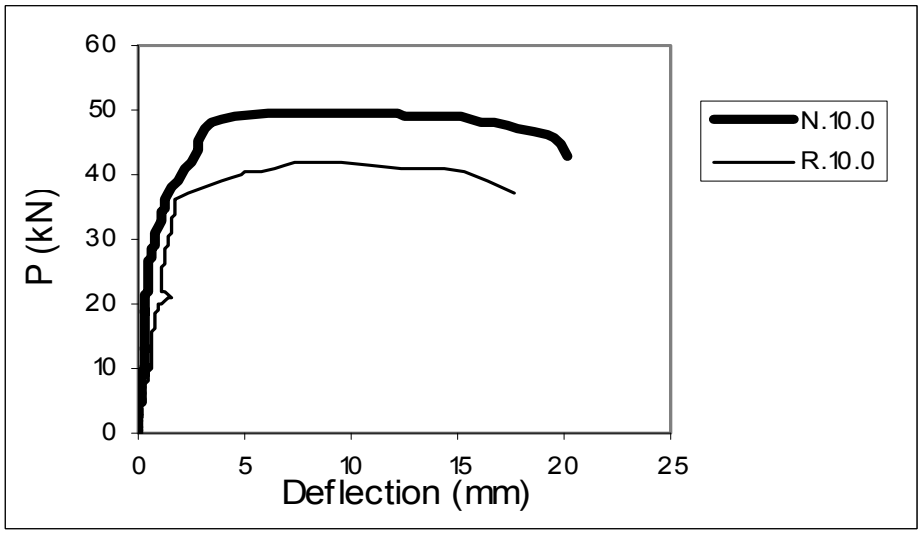

Figure 13: Load versus deflection for N.10.0 and R.10.0 beams.

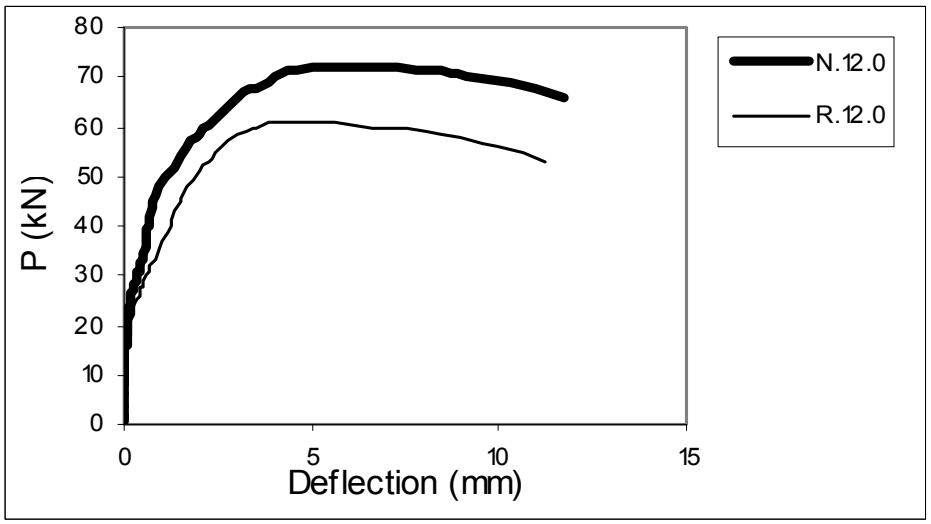

Figure 14: Load versus deflection for N.12.0 and R.12.0 beams.

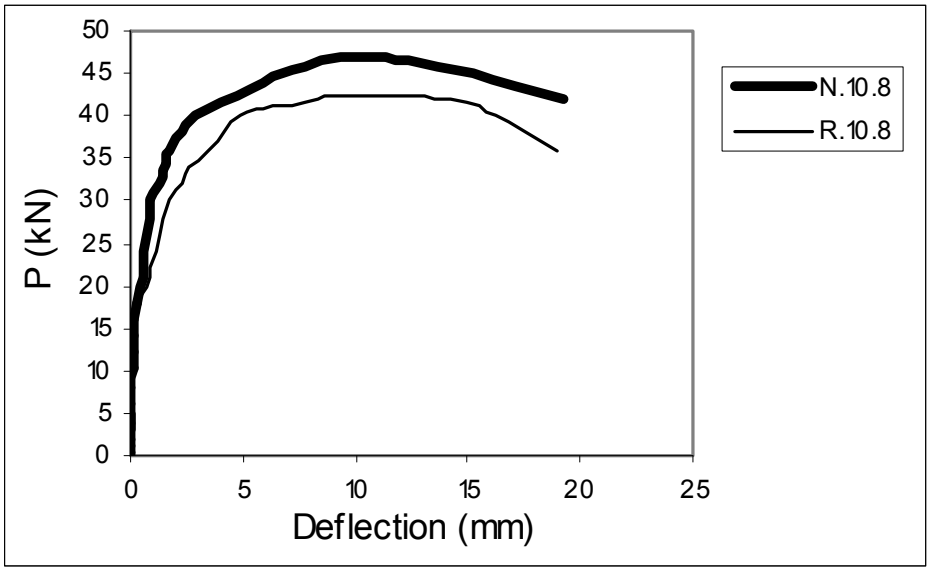

Figure 15: Load versus deflection for N.10.8 and R.10.8 beams.

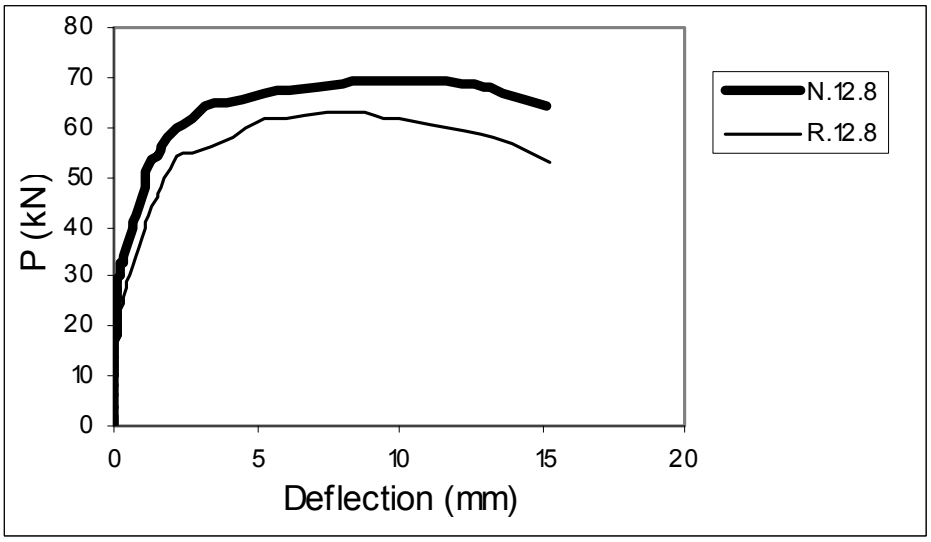

Figure 16: Load versus deflection for N.12.8 and R.12.8 beams.

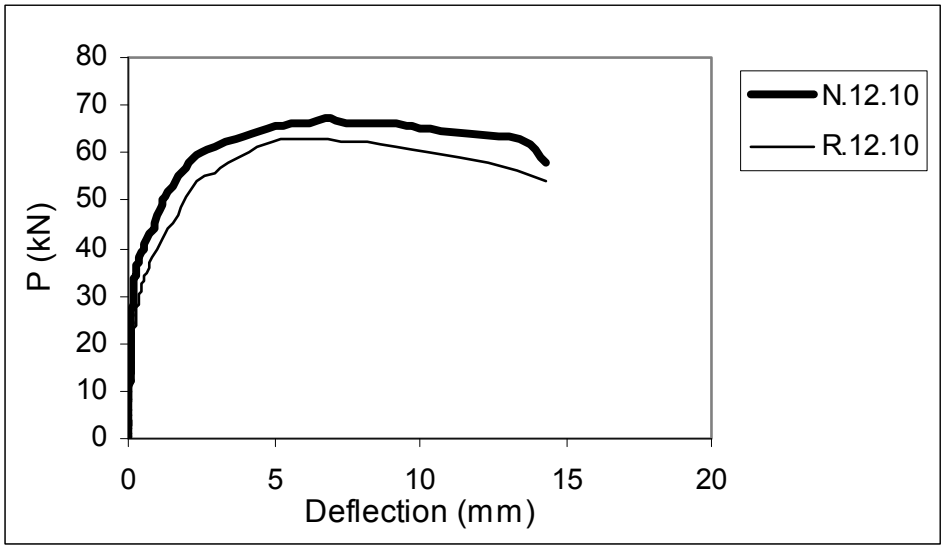

Figure 17: Load versus deflection for N.12.10 and R.12.10 beams.

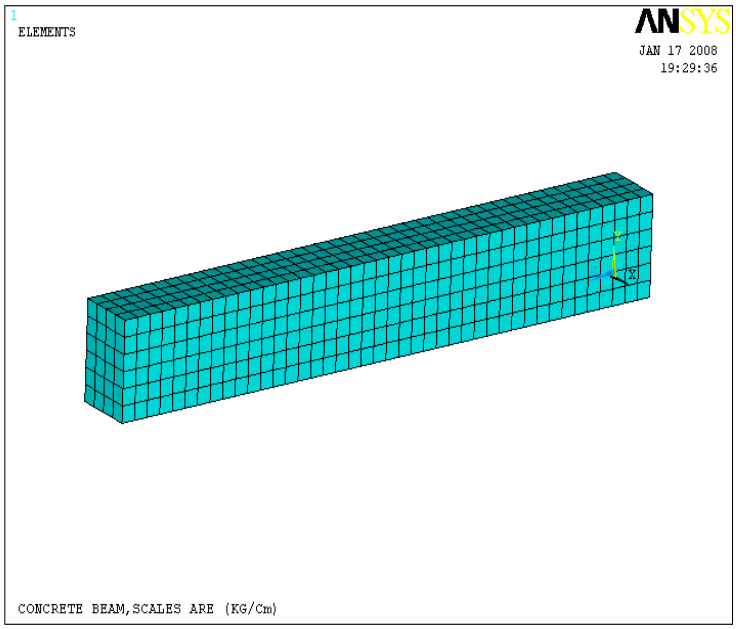

Figure 18: Finite element mesh used for the simulation in ANSYS program.

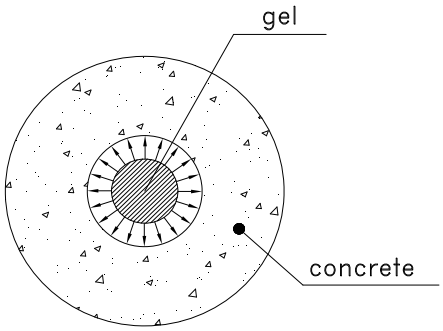

Figure 19: Internal pressures in concrete due to gel swelling.

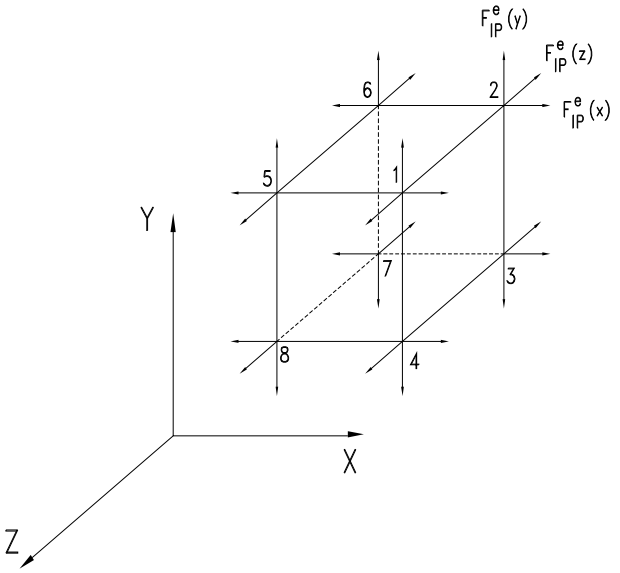

Figure 20: Nodal tensile forces due to internal pressure.

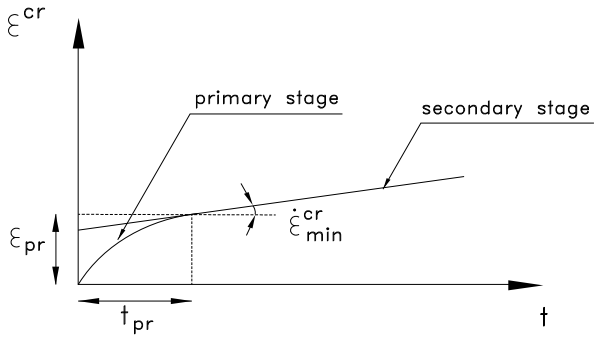

Figure 21: The primary creep and secondary creep stages.

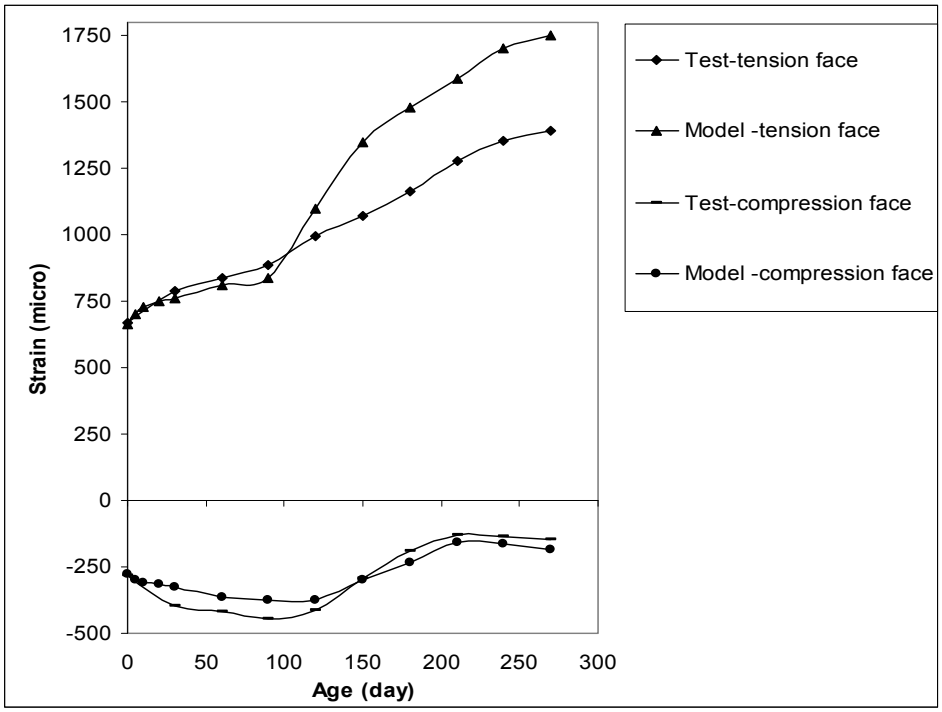

Figure 22: Model results compared to test results for R.8.0 beam.

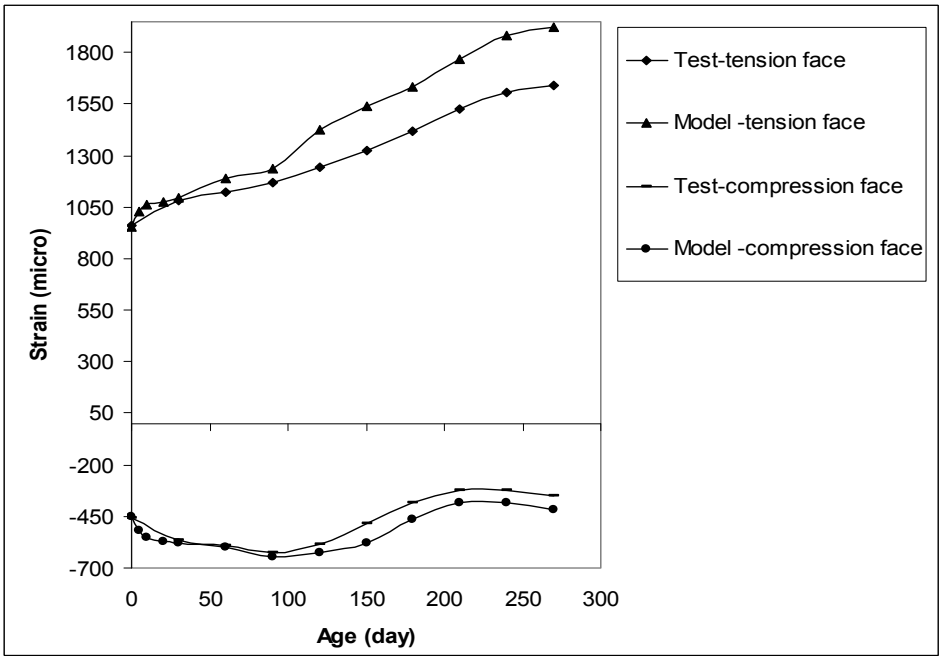

Figure 23: Model results compared to test results for R.10.0 beam.

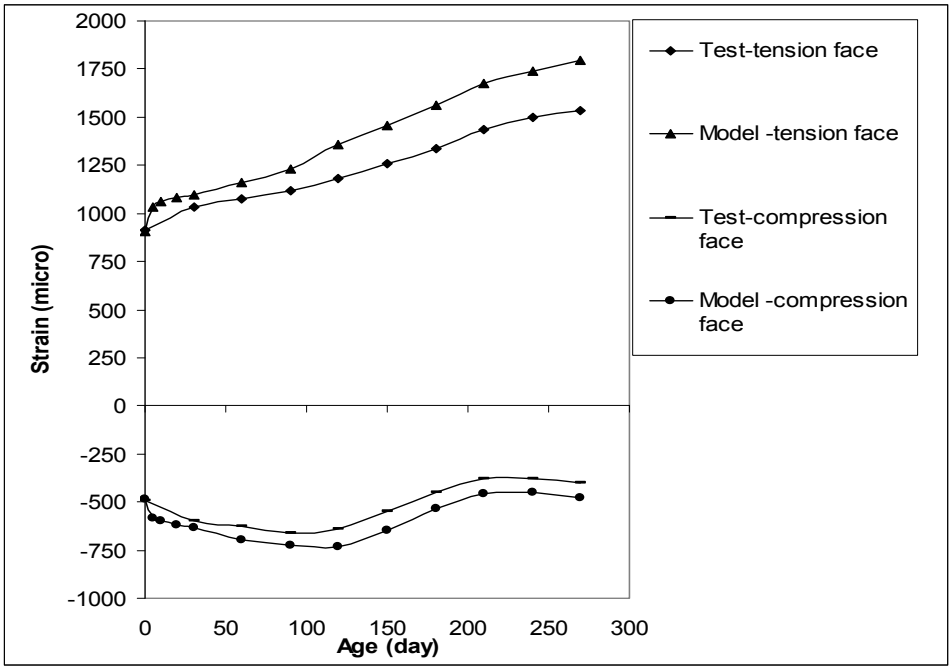

Figure 24: Model results compared to test results for R.12.0 beam.

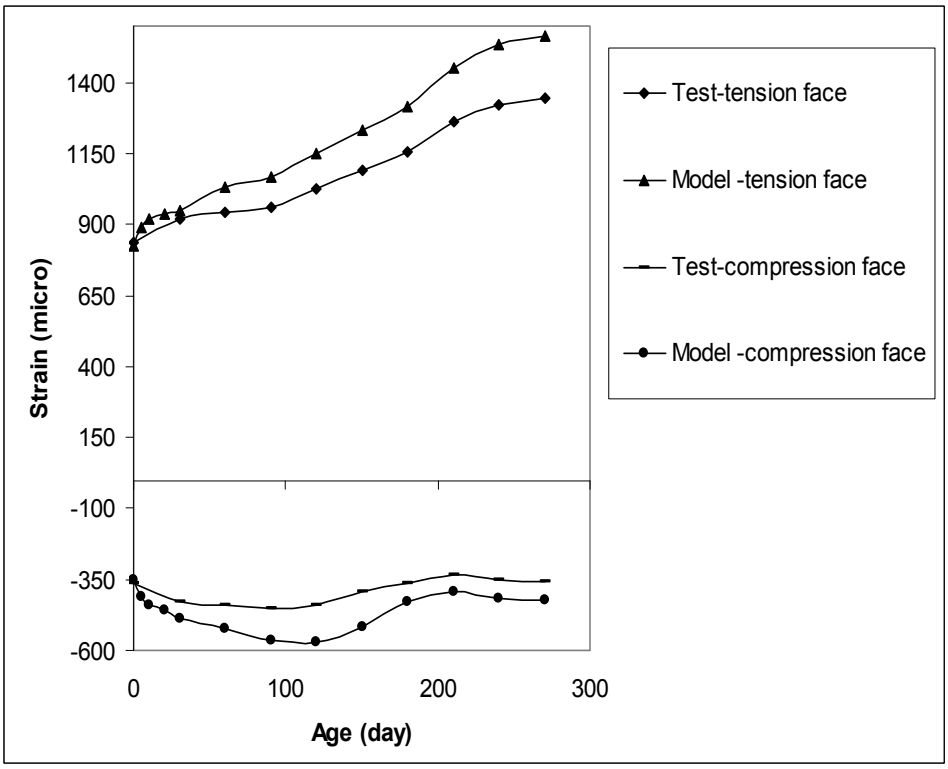

Figure 25: Model results compared to test results for R.10.8 beam.

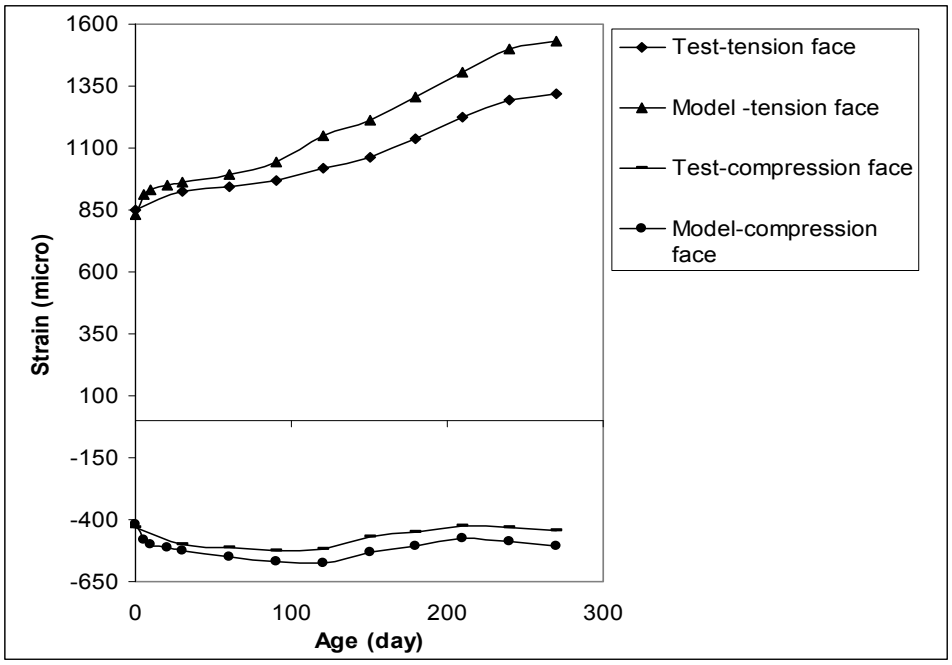

Figure 26: Model results compared to test results for R.12.8 beam.

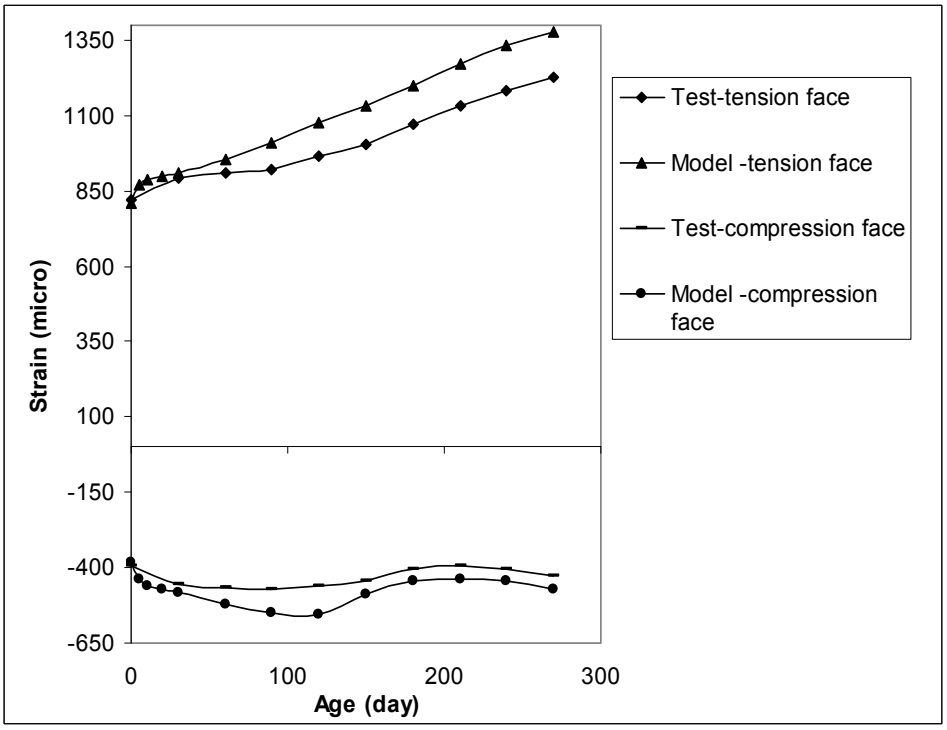

Figure 27: Model results compared to test results for R.12.10 beam.